PERGAMON

International Journal of Solids and Structures 37 (2000) 5493–5504

INTERNATIONAL JOURNAL OF SOLIDS and STRUCTURES

www.elsevier.com/locate/ijsolstr

Experimental determination and empirical representation of out-of-plane displacements in a cracked elastic plate loaded in mode I

Laurent Humbert*, Valéry Valle, Mario Cottron

Université de Poitiers, Laboratoire de Mécanique des Solides, UMR 6610 SP2MI, Boulevard 3, Téléport 2, BP179 8696, Futuroscope Cedex, France

Received 3 December 1998; in revised form 26 April 1999

Abstract

A Michelson interferometer is applied to a mode I fracture mechanic problem to investigate the out-of-plane displacement near the crack tip. For an elastic cracked plate, it appears that the two-dimensional theory predicts correctly the free-stress surface displacement only in a region greater than half the specimen thickness. Combining this two-dimensional solution and the measurements provided by the interferometer, the out-of-plane displacement is likewise accessible inside the previous region where the state of stress is three-dimensional. A mathematical formulation, using an exponential integral function is then proposed to describe the out-of-plane surface displacement in the measurement area around the crack tip.

Keywords: Experimental fracture mechanics; Interferometry; Out-of-place displacement; 3D effects

1. Introduction

In recent years, many studies have been attempted to understand the mechanical behavior of cracked elastic plates, under different loading conditions. Such plates constitute elements of more complex and various elastic structures. Accounting for geometrical singularities like edges or cracks is of great importance in many engineering practices.

Although a realistic mechanical response of these structures, undergoing small displacements, is governed by the equations of the three-dimensional linear elasticity, some simplifying assumptions were

* Corresponding author. Tel.: +33-5-49-49-65-00; fax: +33-5-49-49-65-04.

E-mail addresses: humbert@lms.univ-poitiers.fr (L. Humbert), valle@lms.univ-poitiers.fr (V. Valle), cottron@lms.univ-poitiers.fr (M. Cottron).

0020-7683/00/$ - see front matter
PII: S0020-7683(99)00210-3

made, in the past, to approach this problem. If a two-dimensional view point is therefore adopted, many studies have been performed to determine displacement and stress fields in the neighborhood of the crack tip. Two-dimensional analytical or numerous solutions are moreover available in the literature for plates with moving or stationary cracks of arbitrary shapes (Williams, 1957; Hartranft and Sih, 1977; Bazant and Estenssoro, 1979).

Based on a generalized plane stress theory, in the case of a thin elastic plate which is subjected to in-plane loading, the stresses along the crack front have the well-known inverse square root singularity (Eftis et al., 1977; Sneddon and Lowengrub, 1969). This approximate stress field gives rise to a lateral contraction of the plate which is unbounded. The out-of-plane displacement tends thus to infinity as the distance from the crack tip tends to zero.

Concurrently, experimental studies of fracture mechanics extended their scope using optical methods such as photoelasticity, holography, shadow method, interferometry. These experimental methods, have in some case used and validated the previous theoretical solutions. They have also shown the limitations of the two-dimensional approach. It is specially true for the singular expression of the out-of-plane displacement at the crack tip, which is not, in this fact, in a position to represent a realistic physical quantity very near the crack tip. Twelve years ago, using the method of caustics by reflection, Rosakis and Ravi-Chandar suggested that a two-dimensional field prevails at a distance from the crack tip greater than half the specimen thickness.

Some researchers have jointly investigated the fully three-dimensional stress field arising near the intersection of the crack surfaces and the stress-free border of an elastic plate. Probably due to the abrupt change of boundary conditions at this point (called vertex) and the complex treatment following, few interesting solutions exist for the associated out-of-plane displacement field (Burton et al., 1984; Yang and Freund, 1985). Recently, using Nakamura and Parks numerical results (Nakamura and Parks, 1988), Pfaff et al. have given a mathematical expression for the elastic out-of-plane displacement, which insures a smooth transition to the solution obtained with the generalized plane stress theory (Pfaff et al., 1995). Comparisons have been made afterwards between contour plots of the theoretical form proposed and Michelson interferograms of the out-of-plane surface displacement.

In our paper, the static out-of-plane displacement surface of a plate near the crack tip is evaluated experimentally using Michelson interferometry applied to fracture mechanics in conjunction with theoretical results of the two-dimensional theory. The specimen is loaded in such a way that only mode I loading occurs. This work is moreover limited to plates constituted of elastic and isotropic material. A mathematical formulation including exponential integral functions is then proposed in Section 3 to describe the displacement surface. Comparisons between the previous form and the experimental data are finally performed in the last section.

2. Experimental considerations

For experimental investigations, Michelson interferometer (Born and Wolf, 1980) shown in Fig. 1 is required. A Plexiglas plate, of thickness 8 mm and large in-plane dimensions is used in this experimental set-up. The plate of width 160 mm and height 270 mm contains, through the thickness, a crack of length 60 mm in the middle of the larger side. The specimen is then subjected, at the ends, to a uniform tension normal to the crack plane. For a good reflection of light, the in front surface is covered with a thin aluminum layer (of thickness less than 30 nm). This layer is achieved by putting the undeformed specimen in a vacuum chamber, in which a device vaporizes an aluminum wire onto the specimen faces.

With regard to the interferometer, coherent light from an extended source S is divided at the beamsplitter B into two beams at right angles. They are respectively reflected at a plane mirror M and the specimen surface, and return to B where they are recombined, to be finally recorded further at C by

a CCD camera of sufficient capability. If the difference of optical path between the emergent beams at C is less than the coherent length of the laser (about 3 cm) interference fringes are observed on the monitor screen. In practice, this is achieved when the distance between the virtual surface M′ and the specimen is less than the coherent length of the laser. M′ represents here the symmetrical image of M about B.

The interference pattern provides information at one and the same time, on the surface profile of the specimen and on the orientation of this surface with respect to the mirror M. Generally for an undeformed surface, in the experimental conditions mentioned before, straight line fringes appear indeed on the screen. In fact, the two phenomenon are coupled and the analysis of the interference fringes doesn't give directly the contraction of the specimen surface resulting from the in-plane loading alone. This point will be discussed, in detail, in the next section. (Fig. 2) presents an interferogram of the surface of the loaded specimen realized near the crack tip. The studied area measures approximately 20 mm square and every fringe represents a 257 nm change in elevation. A zoom of the previous image is shown in Fig. 3.

To analyze the fringes, a software, developed in our Laboratory, based on a phase shifting method (Mauvoisin et al., 1991) has been used. According to this method, three recorded images of the interference pattern with different phase shifting are sufficient to determine the profile of the surface plate. Phase shifting is realized from a control device acting on a piezoelectric actuator where the plane mirror M is mounted. Figs. 4 and 5 provide the result of the calculation applied to images similar to these respectively shown in Figs. 2 and 3. The different gray levels indicate the surface profile. In the

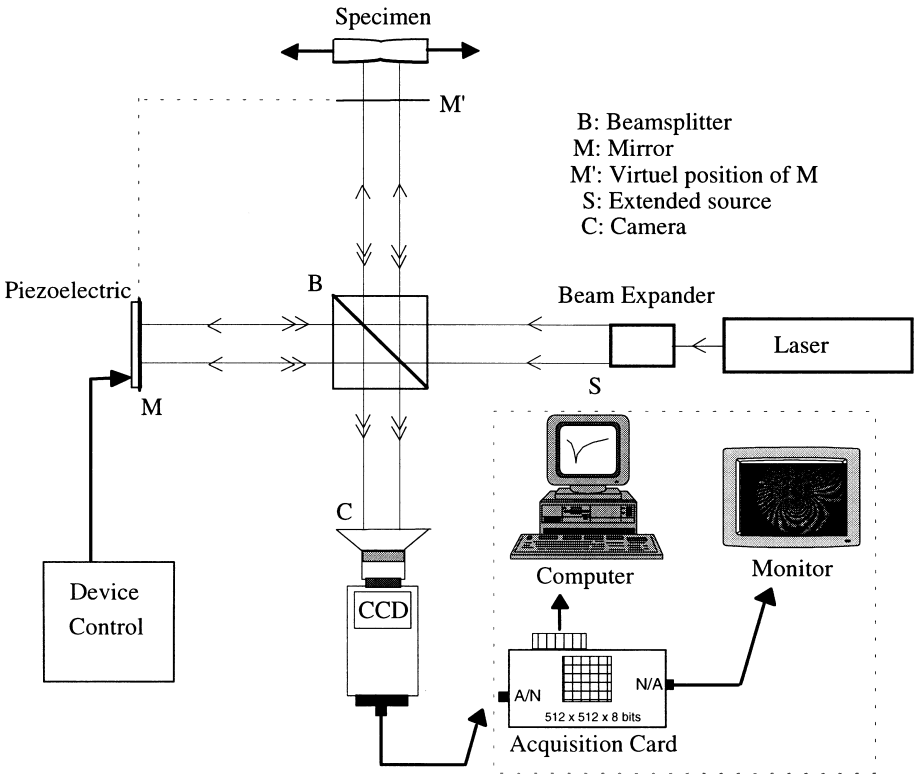

Fig. 1. Michelson interferometer applied to fracture mechanic.

two cases, white areas, which correspond to areas where the fringes are most closely spaced, are points where the calculation is not realized. However, in order to collect information contained in the white area of the large field (Figs. 2 and 4) an enlargement of this field can be performed (Fig. 3) with an adapted lens in front of the CCD camera. The size of the resulting white area (Fig. 5) is then considerably reduced. This practical solution gives the advantage that it does not disturb the interferometric set-up.

3. Out-of-plane displacement determination

3.1. Examination of the experimental measurements

As seen before, the unknown out-of-plane displacement field cannot be reached directly by the data calculated with the software. In fact, they implicitly include the unknown position of the surface plate with respect to the mirror M. For this in the following analysis, the equation of a so-called reference plane, with unknown coefficients, is introduced.

Let us consider now a reference coordinate system (x, y, z) with its origin at the vertex (i.e. the intersection between the crack front and the free-stress border of the plate). The x–y plane corresponds to the free-stress border of the plate (with the x-axis in the continuation of the crack), and the crack front coincides with the z-axis. If the associated cylindrical coordinates (r, θ, z) are rescaled according

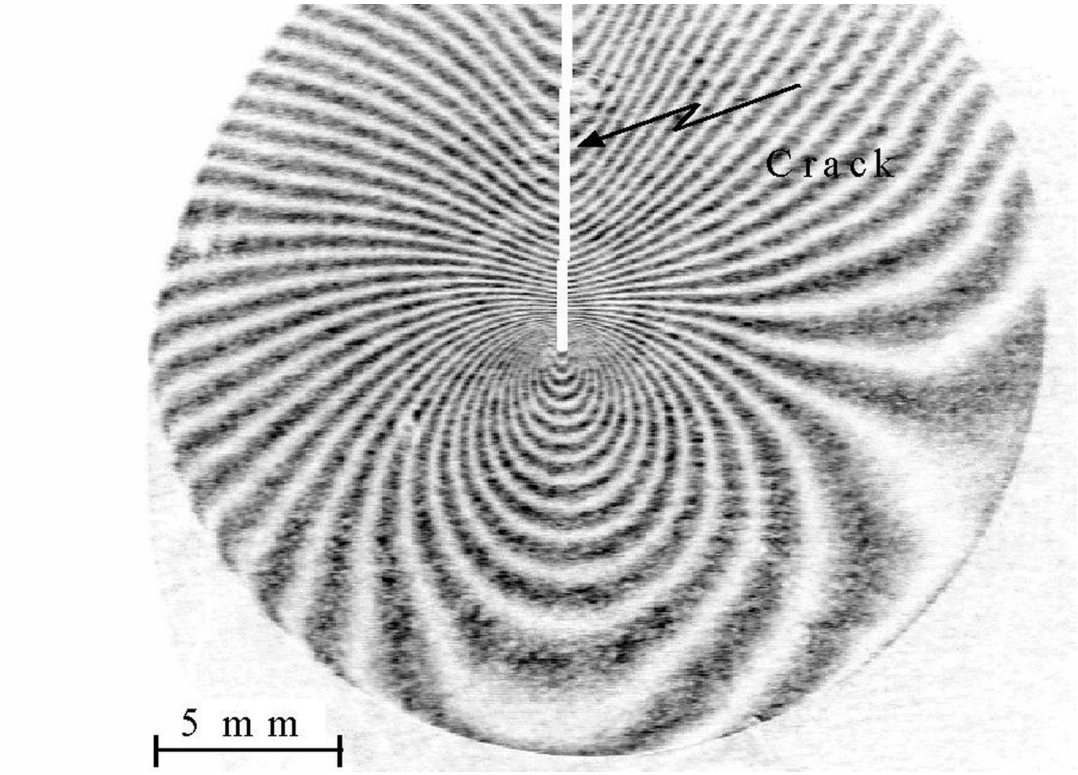

Fig. 2. An interferogram of the out-of-plane surface displacement near the crack tip.

to:

$$(R, \theta, z) = (r/t, \theta, z) \tag{1}$$

where t is the plate thickness, the position of the reference plane, in this new system (R, θ, z) is then represented by:

$$u^{\text{ref}}(R, \theta) = z = p_x R\cos(\theta) + p_y R\sin(\theta) + u_0 \tag{2}$$

The parameter p_x and p_y introduced in Eq. (2) denote respectively, the plane slope with regard to x-axis and y-axis in the coordinate system (R, θ, z). A translation of the reference plane normal to the x–y plane is given by a third parameter u_0.

We assume that in-plane dimensions of the plate are sufficiently large in such a way that a region of essentially two-dimensional plane stress K-field exists outside a near-crack- front three-dimensional field. For such a plate, according to Rosakis (Rosakis and Ravi-Chandar, 1986), a state of generalized plane stress is achieved in a region where $R > 0.5$. The two-dimensional solution is generally expressed by a series expansion (Williams series) about the crack tip. The first term (singular term) corresponds then to the small-scale yielding solution (i.e. the K-field) classically used in a sufficiently small neighborhood of the crack tip. Following the study of Unger (Unger, 1995) about the differences between exact linear elastic solutions and small-scale yielding solutions for crack problems, an estimate of the size of this "K-dominant" region can be rationally given by:

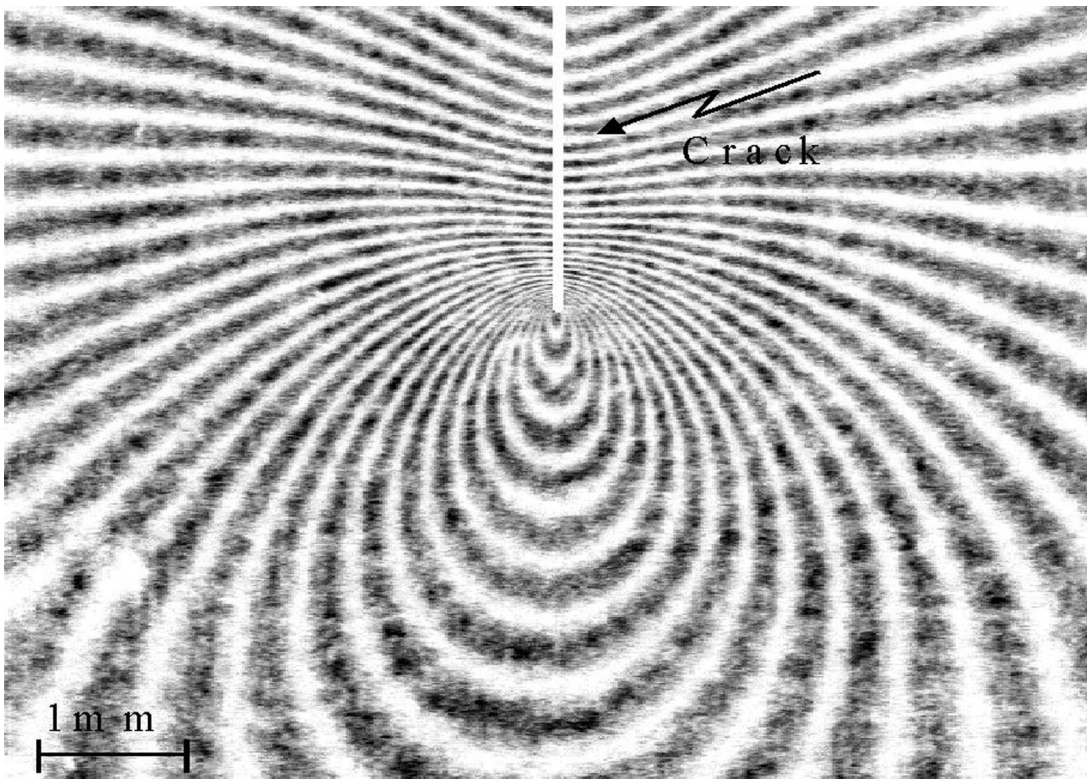

Fig. 3. Zoom of the image Fig. 2.

$$r < \frac{1}{10}L \tag{3}$$

where L represents the crack length. With the in-plane dimensions used for the cracked plate, the K-field is supposed to be dominant if $0.5 < R < 0.8$.

With the previous restrictions and for a mode I loading, the associated out-of-plane displacement is then expressed in the system (R, θ, z) by the expression:

$$u^{\text{pl stress}}(R, \theta) = z = \frac{\nu K t^{0.5} \cos(\theta/2)}{E\sqrt{2\pi R}} \tag{4}$$

where K is the mode I plane stress intensity factor considered here as a parameter. E represents the Young's modulus and ν the Poisson's ratio.

The material of the plate is characterized by a yield stress σ_{ys}, above which it deforms plastically. In other words, there is always a region around the tip of the crack where plastic deformation occurs. With the nondimensional radius R_p, the extent of the plastic zone as a function of θ is given here by (Broek, 1982):

$$R_p = \frac{K^2\left[1 + \frac{3}{2}\sin^2\theta + \cos\theta\right]}{4\pi\sigma_{ys}^2 t} \tag{5}$$

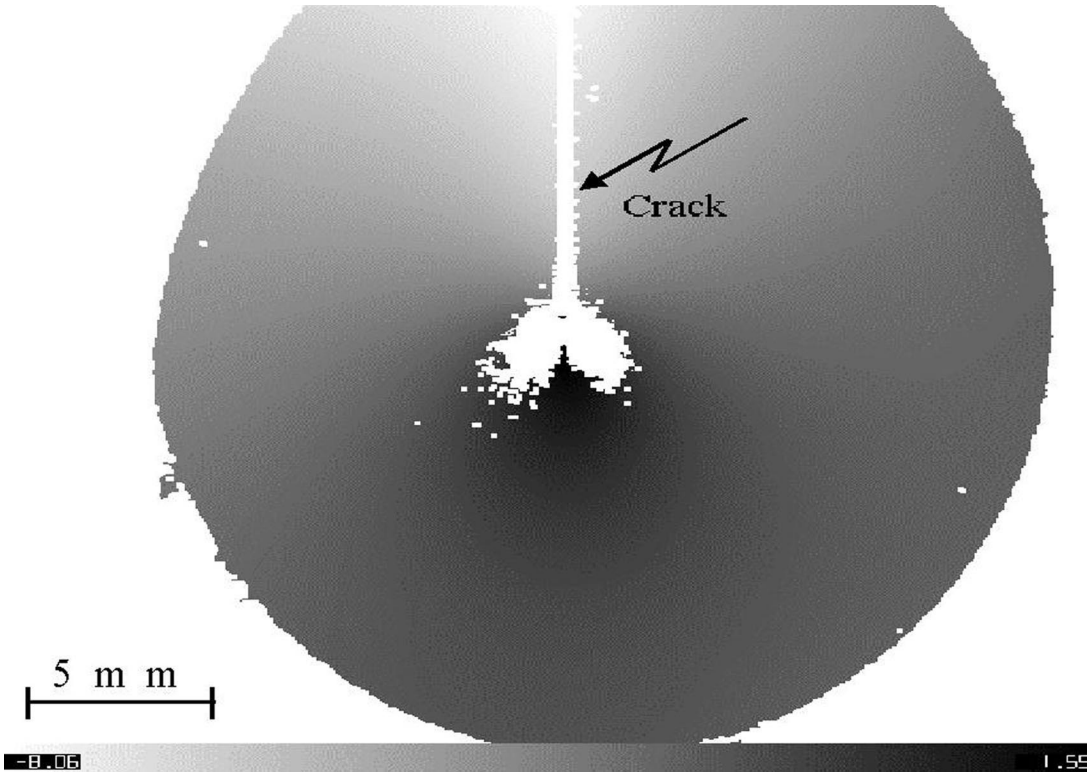

Fig. 4. Result of the calculation for the images similar to the image Fig. 2.

When $0.5 < R < 0.8$, expressions (2) and (4) are finally related to the experimental out-of-plane displacement in this way:

$$u^{\exp}(R, \theta) = u^{\text{pl stress}}(R, \theta) + u^{\text{ref}}(R, \theta) \tag{6}$$

The task is now to determine the four parameters introduced in the right-hand side of Eq. (6). By choosing a set of radii $R \in]0.5; 0.8[$, say M_1, for an angle $\theta_1 \in]0; \pi[$, a vector $\underline{\mathbf{B}}_1$ with M_1 elements $u^{\exp}(R_i, \theta_1)$ is created ($i = 1, \ldots, M_1$). Corresponding to the vector $\underline{\mathbf{B}}_1$, a matrix $\mathbf{A}_1$ with $M_1 \times 4$ elements is obtained by using the right-hand side of Eq. (6). If this procedure is repeated with N angles θ_j linearly distributed in the range $]0; \pi[$, a set of N vectors $\underline{\mathbf{B}}_j$ and N matrix $\mathbf{A}_j$ are available ($j = 1, \ldots, N$). The previous sub-vectors $\underline{\mathbf{B}}_j$ and sub-matrix $\underline{\mathbf{A}}_j$ are then joined to form respectively, a vector $\underline{\mathbf{B}} = (\underline{\mathbf{B}}_1, \underline{\mathbf{B}}_2, \underline{\mathbf{B}}_3, \ldots, \underline{\mathbf{B}}_N)^{\mathrm{T}}$, with $M = (\sum_{j=1}^{N} M_j)$ elements and an associated matrix $\mathbf{A}$ containing $M \times 4$ elements:

$$\mathbf{A} = \begin{pmatrix} \mathbf{A}_1 \\ \mathbf{A}_2 \\ \mathbf{A}_3 \\ \cdots \\ \mathbf{A}_N \end{pmatrix}$$

The problem is thus reduced to solve the following overdetermined linear system:

$$\mathbf{A}\underline{\mathbf{X}} = \underline{\mathbf{B}} \tag{7}$$

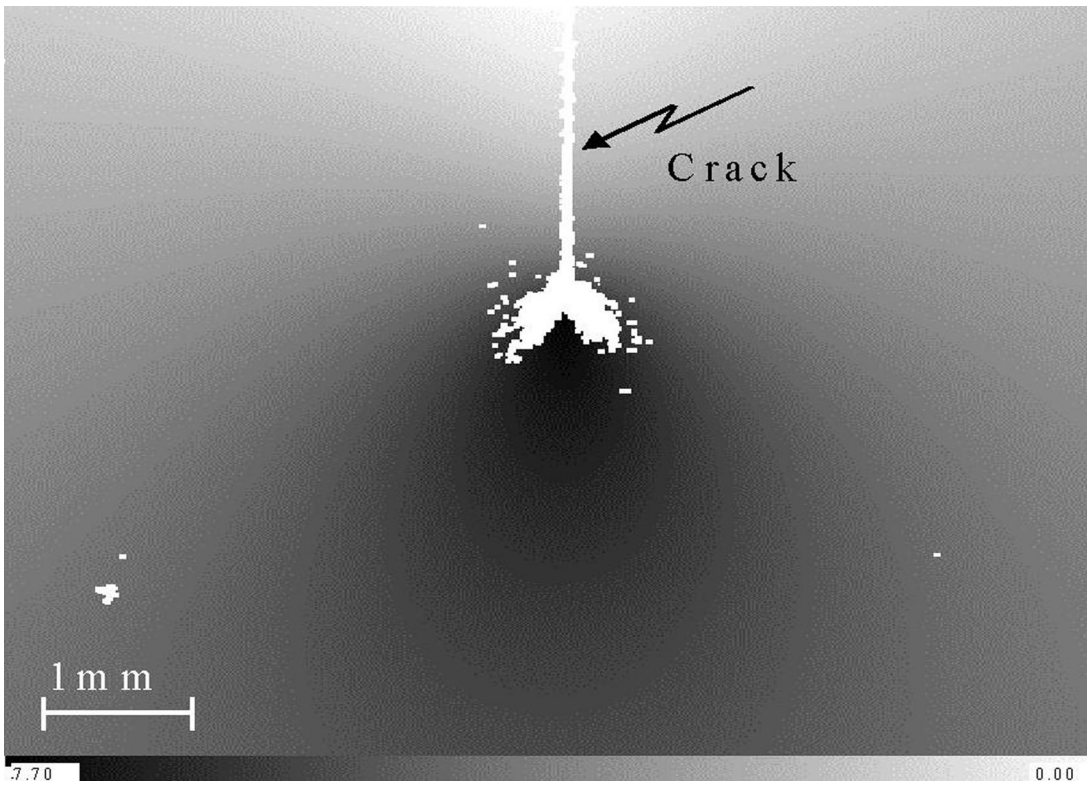

Fig. 5. Corresponding calculation for the zoomed image Fig. 3.

Table 1
Numerical values calculated for the parameters of the reference plane and the mode I plane stress intensity factor

p_x (mm)	p_y (mm)	u_0 (mm)	K in MPa $\sqrt{\text{mm}}$
−0.00117	−0.000163	−9.82*E*-5	28.53

where $\underline{\mathbf{X}}$ is the unknown vector containing the four parameters p_x, p_y, u_0 and K. The solution of the set of simultaneous Eq. (7), with $N = 10$, is shown in Table 1. In this case, M is equal to 785. In the calculation, the numerical values used for the Young's modulus and the Poisson's ratio are respectively, 3 GPa and 0.37.

Moreover, taking 50 MPa for the yield stress and the numerical value calculated previously for K, Eq. (5) allows us to estimate the size of the plastic region. With the nondimensional radius R_p, it is found that the maximal extent of the inelastic region is equal to 0.0065 and is very small compared to the elastic region. Fig. 6 gives a relative measure of the characteristic size of the elastic and plastic regions.

With the numerical values from Table 1 for the four parameters and the results given by the software, the difference $(u^{exp} - u^{ref})$ is represented in Fig. 7 by small circles, for different angles θ. The plots with continuous lines in the figure indicate the two-dimensional out-of-plane displacement for the same angles. As expected, when $R > 0.5$, good agreement is observed between the two-dimensional representation of the displacement and the corresponding plot of the expression $(u^{exp} - u^{ref})$. In fact, one notices that the difference $(u^{exp} - u^{ref})$ gives naturally the out-of-plane displacement due to the in-plane loading, and this, in all the region surrounding the crack tip (i.e. when $0 < R < 0.8$).

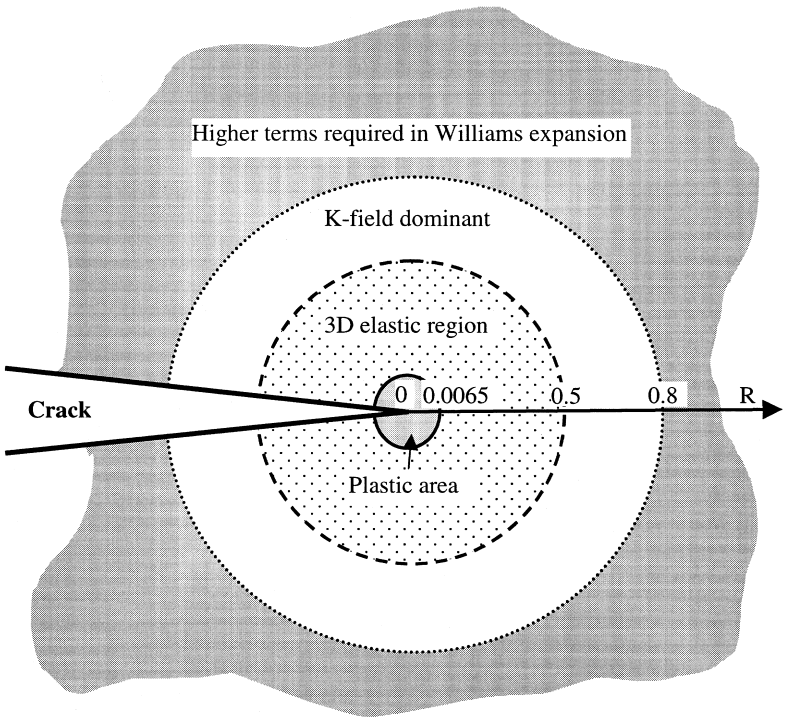

Fig. 6. Relative sizes of the elastic and plastic regions.

3.2. Theoretical expression

The previous results will serve us now to give a mathematical representation of the three-dimensional out-of-plane displacement near the crack tip. With the system (R, θ, z) again, we propose to explain the out-of-plane displacement $(u^{\exp} - u^{\text{ref}})$ with the following equation:

$$u^{3d}(R, \theta) = z = \frac{Kt^{0.5}\nu}{E}\left[bE_i\big(2, a(\theta)R\big) + \cos(\theta/2)(1 - e^{-cR})\frac{1}{\sqrt{2\pi R}}\right] \tag{8}$$

where b, c are unknown constants and $a(\theta)$ an unknown function of θ. E_i is an exponential integral function expressed explicitly as:

$$E_i(2, R) = \int_1^{\infty} \frac{e^{-Rt}}{t^2}\,\mathrm{d}t, \quad R > 0 \tag{9}$$

Using mathematical properties of the exponential integral functions (EIF) (Abramowitz and Stegun, 1965), Eq. (8) insures a smooth transition to the out-of-plane displacement field from the plane stress approximation (see Eq. (4)). This is achieved practically when $R > 0.5$. In addition, EIF provide finite values for the expression (8), when R tends to zero.

To determine the constants b, c and the function $a(\theta)$, the following system of equations is considered for $\theta = 0$:

$$f_i(a, b, c) = u^{3d}(a, b, c, R = R_i, \theta = 0) - (u^{\exp} - u^{\text{ref}})(R = R_i, \theta = 0) = 0, \quad i = 1, \ldots, n \tag{10}$$

where $0 < R_1 < R_2 < R_3 < \cdots < R_n < 0.8$. R_i represent here the abscises of n points deriving from the previous plot shown in Fig. 7 (when θ is equal to 0). Thus, minimization methods like Newton method

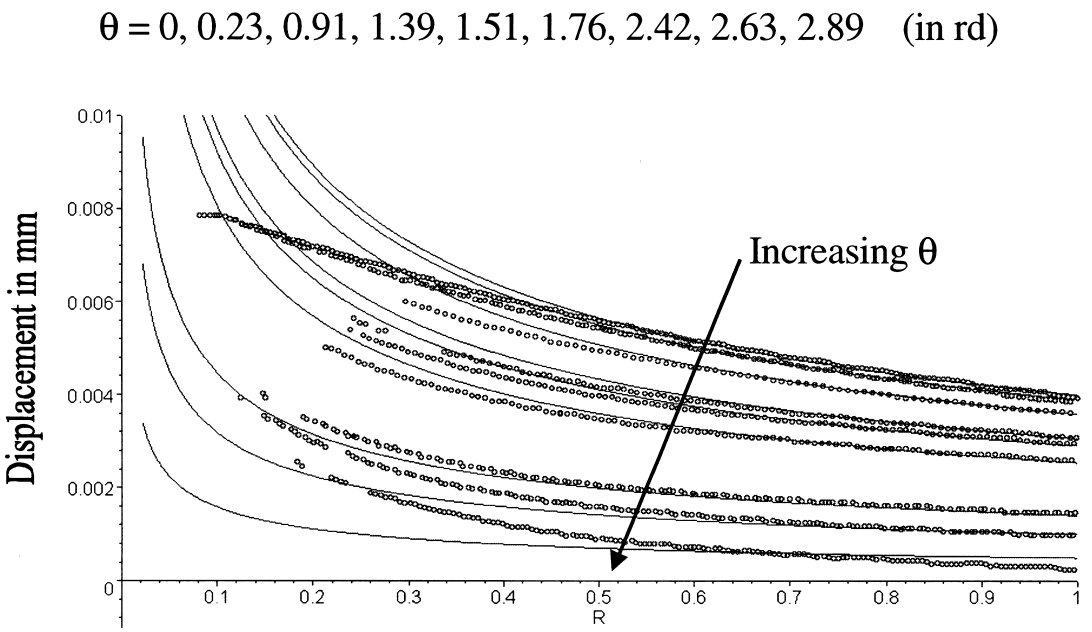

Fig. 7. Evolution of the experimental out-of-plane displacement for different angles θ.

Table 2
Numerical values found for the parameters when $\theta = 0$

$a(\theta = 0)$	b	c
9.186	0.787	7.335

Table 3
Evolution of the parameter a for $\theta \in [0, \pi[$ (the values are the same in the range $]-\pi, 0]$)

θ (rd)	0	0.23	0.91	1.39	1.51	1.76	2.42	2.63	2.89
$a(\theta)$	9.18	8.98	8.43	7.68	7.40	6.97	5.44	4.68	4.06

can be applied to reach a local minimum of the function:

$$F(x) = \sum_{i=1}^{n} f_i^2(x), \quad x = a, b, c$$

With appropriate initial value, the method converges very well to a solution presented in Table 2. With the knowledge of the coefficients b and c, similar calculations are started again with the only unknown coefficients a, for different angles θ in the range $]-\pi, \pi[$ (see Table 3). Finally, using a classical interpolation technique, it is found that the evolution of $a(\theta)$ is represented by the following even function of θ, in the range $]-\pi, \pi[$:

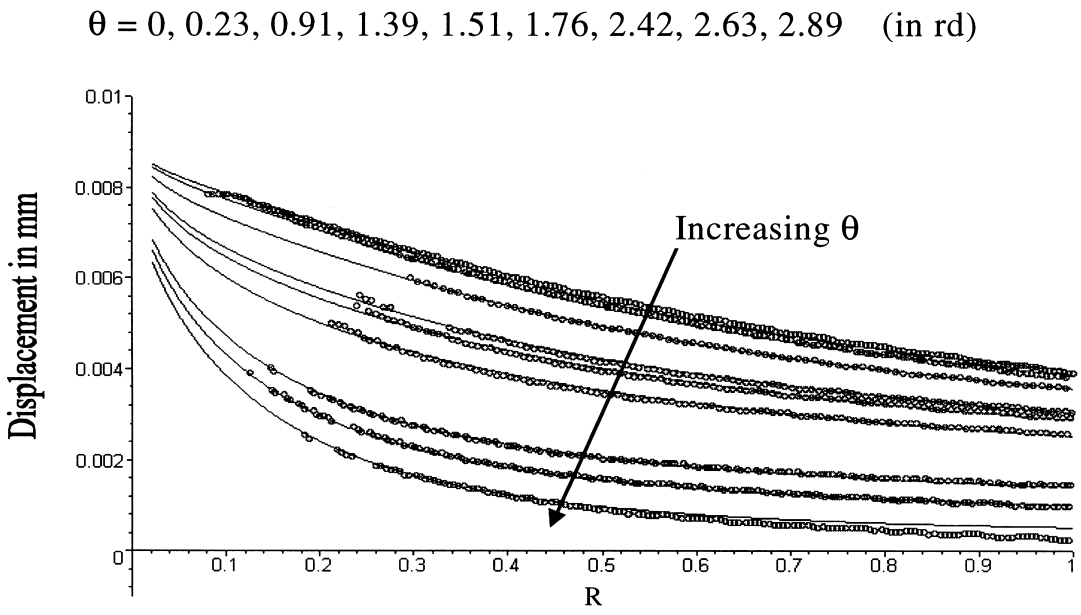

Fig. 8. Representation of the theoretical expression (8) for different angles θ (continuous lines).

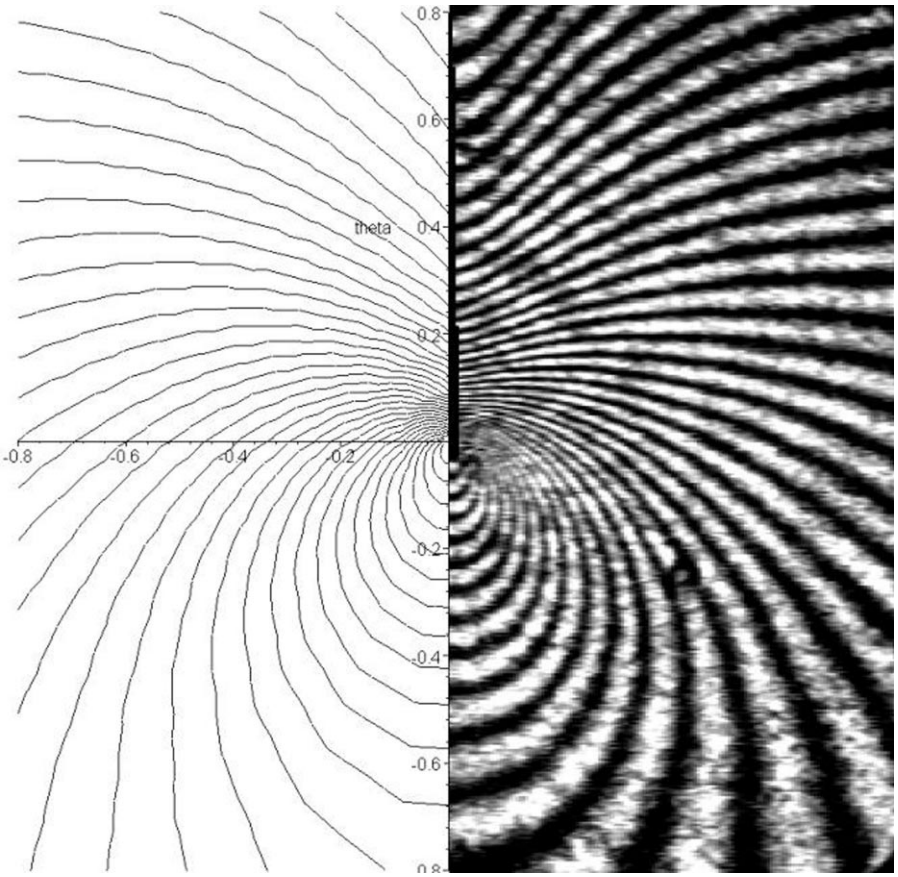

Fig. 9. Simulation of interference fringes.

$$a(\theta) = a_1 \cos(\theta/2) + a_2$$

$$a_1 = 5.73$$

$$a_2 = 3.32 \tag{11}$$

It should be noted that the number of the points used and their positions influence the values of the previous parameters. In practice, we take the 25 closest points to the crack tip. With the values of Table 2 for b and c, Eq. (8) combined with Eq. (11) give monotonic and bounded functions of R in the range $[0, \infty[$, $\forall\theta \in]-\pi, \pi[$. Such functions are represented in Fig. 8 for the angles θ given in Table 3. Good agreement is observed between the discrete values obtained before and the plot of the theoretical form proposed in this section.

A simulation of fringes is performed by using the expression (6), in which Eqs. (8) and (11) take the place of $u^{\text{pl stress}}$. Good agreement is observed in Fig. 9 between simulated and experimental fringes in the region near the crack tip, thus validating the previous analysis.

4. Conclusion

An hybrid method combining interferometry with theoretical results of the two-dimensional theory is presented to determine the out-of-plane displacement in the fully three-dimensional region near the crack tip. This method is achieved for elastic cracked plates with in-plane dimensions sufficiently large to allow the existence of a plane stress field surrounding the three dimensional region. According to this study, the global out-of-plane displacement field u^{exp} measured by interferometry results from the orientation changing of the plate, described by a reference plane u^{ref} and the out-of-plane displacement u^{3d} only due to the in-plane loading (Poisson's effect). The equation of the plane is determined in such a way to shift the experimental data, deriving from the interferometry, to the theoretical curves available in the two-dimensional region. A new theoretical expression, using an exponential integral function, is also proposed to describe the unadulterated out-of-plane displacement everywhere near the crack tip.

Finally, from the mathematical form of the global displacement field, fringes are simulated and compared to fringes obtained experimentally. As shown in Fig. 8, this new approach appears to predict correctly, the out-of-plane displacement in all the region near the crack tip. Other tests should be realized on other elastic materials to refine the parameters introduced in the previous equations. The generality of the expression (8) for linear elastic mode I cracking problems should be then confirmed. An extension of this work is envisaged for crack problems under mixed mode I–mode II loading.

References

Abramowitz, M., Stegun, I.H., 1965. Handbook of Mathematical Functions. Dover, New York.

Bazant, Zdenek P., Estenssoro, Luis F., 1979. Surface singularity and crack propagation. Int. J. Solids Structures 15, 405–426.

Born, M., Wolf, E., 1980. Principles of Optics, 6th ed. Pergamon Press, New York.

Broek, D., 1982. Elementary Engineering Fracture Mechanics. The Hague, The Netherlands, Martinus Nijhoff 3rd revised edition.

Burton, W.S., et al., 1984. On the implications for LEFM of the three-dimensional aspects in some crack/surface intersection problems. International Journal of Fracture 25, 3–32.

Eftis, J., et al., 1977. Crack border stress and displacement equations revisited. Engineering Fracture Mechanics 9, 189–210.

Hartranft, R.J., Sih, G.C., 1977. Stress singularity for a crack with an arbitrarily curved front. Engineering Fracture Mechanics 9, 705–718.

Mauvoisin, G., Bremand, F., Lagarde, A., 1991. Improvement on phase shifting method precision and application on shadow moir method. In: Proc. of Moir Techniques, Holographic Interferometry, Optical NDT and Applications to Fluid Mechanics, SPIE, San Diego 1554 B, 181–187.

Nakamura, T., Parks, D.M., 1988. Three-dimensional stress field near the crack front of a thin elastic plate. J. Appl. Mech 55, 805–813.

Pfaff, R.D., et al., 1995. An interpretation of Twyman-Green interferograms from static and dynamic fracture experiments. Int. J. Solids Structures 32, 939–955.

Rosakis, Ares J., Ravi-Chandar, K., 1986. On crack-tip stress state: an experimental evaluation of three-dimensional effects. Int. J. Solids Structures 22, 121–134.

Sneddon, I.N., Lowengrub, M., 1969. Crack Problems in the Classical Theory of Elasticity. Wiley, New York.

Unger, David, J., 1995. Analytical Fracture Mechanics. Academic Press, New York.

Yang, W., Freund, L.B., 1985. Transverse shear effects for through-cracks in an elastic plate. Int. J. Solids Structures 9, 977–994.

Williams, M.L., 1957. On the stress distribution at the base of a stationary crack. J. Appl. Mech 24, 109–114.